Measurement of the Proton Wave Function in Molecular Hydrogen by Neutron Compton Scattering

J. Mayers

Rutherford Appleton Laboratory, Chilton, OX11 0QX, England
(Received 21 June 1993)

The momentum distribution of the proton in liquid and solid hydrogen has been measured by neutron Compton scattering (NCS), at energy transfers between 3 and 50 eV. The data display features due to interference between the proton and neutron wave functions and are accurately described by a simple quantum mechanical model, incorporating previous spectroscopic data. The excellent agreement between calculation and data in this simple system demonstrates that the NCS technique can provide accurate information about the behavior of the proton in condensed matter. There are many applications of NCS to more complex physical systems of fundamental interest in physics, chemistry, and biology.

The possibility of measuring nuclear momentum distributions in condensed matter systems by neutron scattering was first suggested by Hohenberg and Platzmann [1] nearly 30 years ago. The method is analogous to the measurement of electron momentum distributions by Compton scattering [2] and measurement of nucleon momenta by deep inelastic scattering [3] and is known as neutron Compton scattering (NCS) or deep inelastic neutron scattering (DINS). The theoretical basis of all three techniques is the impulse approximation (IA), which is exact when the momentum transfer **q** and energy transfer ω are infinite [4–6]. When the IA is valid, the scattering cross section is proportional to the distribution of nuclear momentum components along the direction of **q** and can be used to determine $n(\mathbf{p})$, the distribution of nuclei (and hence atoms) in momentum space.

NCS measurements on protons have a particularly simple interpretation, as the interaction of protons with other atoms can usually be accurately accounted for [7,8] in terms of a single particle potential and hence by a proton wave function. From elementary quantum mechanics, $n(\mathbf{p})$ is related to the Fourier transform of the proton wave function $\Psi(\mathbf{r})$ via

$$n(\mathbf{p}) = \frac{1}{(2\pi)^3} \left| \int \Psi(\mathbf{r}) \exp(i\mathbf{p}\cdot\mathbf{r}) \, d\mathbf{r} \right|^2 , \tag{1}$$

and an NCS measurement of $n(\mathbf{p})$ can be used to determine the wave function in an analogous way to the determination of real space structure from a diffraction pattern. In principle such measurements can provide very detailed information about the behavior of the proton in a variety of systems of fundamental interest in physics, chemistry, and biology.

NCS measurements on protons have only become possible since the construction of intense accelerator based neutron sources, which have allowed accurate inelastic neutron scattering measurements with energy transfers in the 1 eV region [9]. For NCS measurements on the proton in molecular hydrogen, energy transfers much greater than the vibrational frequency of the molecule (516 meV [10]) are required before the IA can be used to reliably determine $n(\mathbf{p})$. At lower energy transfers the IA is no

longer valid and $n(\mathbf{p})$ is not related in a simple way to the observed scattering intensities. In systems with weaker binding, lower energy transfers can be used and many early NCS measurements were performed on helium at relatively low energy and momentum transfers ($\omega < 300$ meV and $q < 15$ Å^{-1}). These studies were motivated primarily by the possibility of directly observing the Bose condensate fraction in superfluid ^{4}He [11–15]. More recently NCS measurements with $15 < q < 40$ Å^{-1} and incident energies up to 2 eV have been made on condensed phases of helium [16] and neon [17]. There have been a few pioneering studies on various systems at 1 eV energy transfers [18–20]. Measurements on molecular hydrogen have also been made, with ω insufficient to excite vibrational transitions [21,22]. This allows a measurement of the center of mass motion of H_2 molecules rather than the momentum distribution of individual protons. The measurements described here were made with $3 < \omega < 50$ eV and $30 < q < 130$ Å^{-1}. At such high values of q and ω, accurate NCS measurements can be made even in strongly bound systems such as hydrogen.

The formal statement of the IA in neutron scattering is [23]

$$S(\mathbf{q},\omega) = \int n(\mathbf{p}) \delta \left[\omega + \frac{p^2}{2M} - \frac{(\mathbf{p}+\mathbf{q})^2}{2M} \right] d\mathbf{p} , \tag{2}$$

where $S(\mathbf{q},\omega)$ is the dynamic structure factor, $n(\mathbf{p})$ is the nuclear momentum distribution, **p** is the atomic momentum, and M is the nuclear mass. The δ function expresses the conservation of kinetic energy, which applies to the collision between the nucleus and the neutron when the IA is satisfied. When the scattering sample is isotropic it can be shown that [5]

$$S(q,\omega) = (M/q)J(y) , \tag{3}$$

where

$$y = (M/q)[\omega - q^2/2M] \tag{4}$$

and

$$J(y) = 2\pi \int_{|y|}^{\infty} p n(p) \, dp . \tag{5}$$

$J(y)dy$ is the probability that an atom has a momentum

component along $\mathbf{q}$ with magnitude between y and $y+dy$ and is known as the Compton profile. Equations (3)–(5) express the "y scaling" property of the neutron cross section at sufficiently high q [24].

The measurements were performed on the electronvolt spectrometer (EVS) at the ISIS neutron source [25]. A filter difference technique [26], with a gold foil analyzer, was used to fix the energy of the scattered neutron at 4.922 eV. Time of flight techniques [27] were used to determine the energy of the scattered neutron and hence $S(q,\omega)$. The sample of parahydrogen was measured at temperatures of 20 and 4 K (the liquid and solid phases, respectively) and was a 5% scatterer, contained in a planar aluminum can with a sample thickness of ~ 1 mm and with the sample plane perpendicular to the incident beam. Measurement times were 24 h at each temperature. Because of the y scaling property mentioned above, all scans through q,ω space map onto the same function $J(y)$. Thus, providing the IA is well satisfied, the measurements of $J(y)$ at different angles differ only in the width of the instrument resolution function and can be averaged to improve statistical accuracy. As the differences observed between the 4.9 and 20 K data were at the limits of measurement accuracy, the data sets at the two temperatures were also averaged to further reduce the statistical error.

Figure 1(a) shows the average of Compton profiles measured in ten ^{3}He gas detectors at angles between 35° and 45°, 1(b) that for ten detectors between 45° and 55°, and 1(c) for twenty detectors at angles between 55° and 75°. The instrument resolution function [25,28] is also shown for each of these data sets, together with the energy and momentum transfers corresponding to the detector at the center of each bank. There is a small multiple scattering component in the data which is visible at large positive y values, particularly in the data sets at the two lower angles, and this has been fitted by a second-order polynomial.

It follows from the physical significance of the Compton profile that $J(y)$ should be symmetric about $y=0$. However, the data in Fig. 1 show small systematic shifts of the peak of the distribution towards negative y, due to inaccuracies in the IA which are present at the finite q of the measurement. It has been shown by Sears [5] that symmetrization of data about $y=0$ removes most of these inaccuracies and this procedure has been followed to produce the data shown in Fig. 2. The data from all detectors between 35° and 55° has been averaged and the multiple scattering background subtracted before symmetrization.

The results are well described by a simple quantum mechanical model. It is assumed that the hydrogen molecule is bound by a harmonic potential and that its center of mass translational motion is independent of its vibration along the bond axis. The latter approximation is highly accurate due to the different energy scales involved in the two types of motion. $J(y)$ is then the convolution
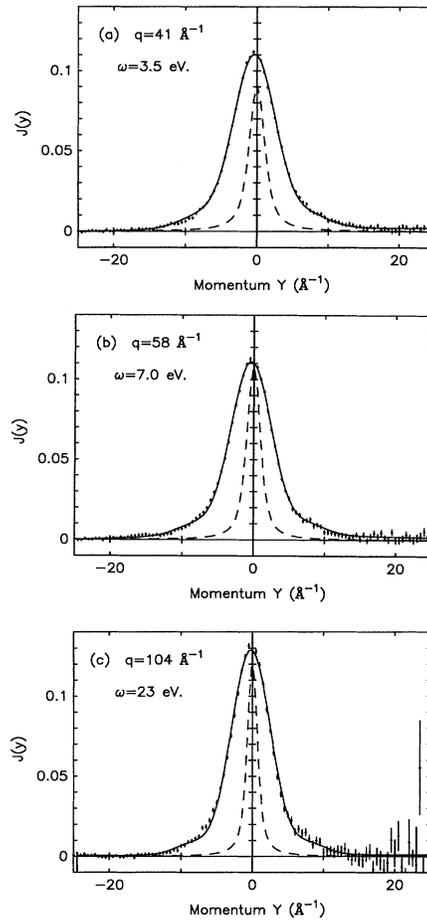
FIG. 1. The data points are the average of the measured neutron Compton profiles obtained from detectors in three different angular ranges: (a) 35°–45°, (b) 45°–55°, and (c) 55°–75°. The solid line is the fit described in the text. The resolution function is shown for each data set as a dashed line.

of the momentum distributions for the vibrational and translational motions considered separately,

$$J(y) = \int J_T(y')J_V(y'-y)dy'. \tag{6}$$

The translational momentum distribution $J_T(y)$ is approximated by a Gaussian function,

$$J_T(y) = \frac{1}{\sqrt{2\pi\sigma_T^2}}\exp\left[\frac{-y^2}{2\sigma_T^2}\right]. \tag{7}$$

From previous measurements [21] the kinetic energy of the center of mass motion is 63 ± 6 K in the liquid at 17 K and 76 ± 9 K in the solid at 10 K. Taking the average of these values as 70 K, the translational kinetic energy of each atom is 35 K $=3\sigma_T^2/(2M)$ and $\sigma_T=0.70$ Å^{-1}.

The momentum distribution $J_V(y)$ associated with vibration along the bond can be determined from the wave function of the proton in the molecule. Since the binding
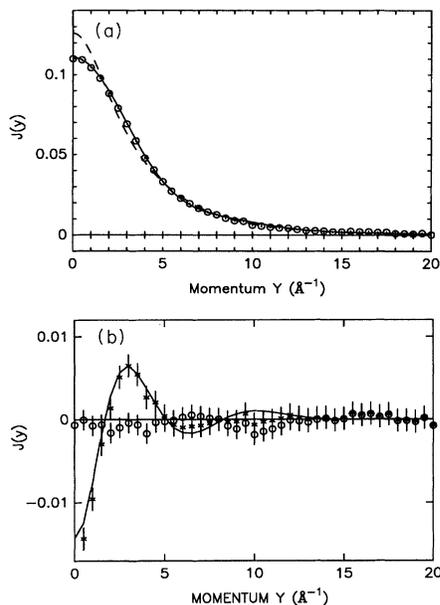
FIG. 2. In (a) the points O are the sum of data from twenty detectors at scattering angles between 35° and 55° after subtraction of multiple scattering and symmetrization. The solid line is the calculation using Eq. (9) and the dashed line that using Eq. (10), both after convolution with the instrument resolution function. (b) The difference between the data and the two models: O, Eq. (9); ×, Eq. (10). The solid line is the difference between the quantum and classical models.

FIG. 3. The solid line is the $J_V(y)$ calculated from Eq. (9); the dotted line is the convolution of $J_V(y)$ and $J_T(y)$, i.e., $J(y)$ of Eq. (6). The dashed line is the convolution of $J(y)$ with the instrument resolution function used in Fig. 2.

is assumed harmonic, each atom will have a Gaussian probability distribution along the bond axis, centered at its mean position at distance R from the center of mass, where $2R$ is the bond length. In parahydrogen below 20 K only the $J=0$ state of rotation is thermally occupied and the molecular wave function has no directional dependence. Thus the wave function of each proton is a spherical shell

$$\Psi(r) = [2\pi^{3/2}\sigma(\sigma^2+2R^2)]^{-1/2}\exp\left[\frac{-(r-R)^2}{2\sigma^2}\right], \quad (8)$$

where the mean square displacement of the atom from its mean position along the bond is $\sigma^2/2$ ($=\int r^2|\Psi(r)|^2 dr$). The normalization constant in Eq. (8) is approximate in that it relies upon the shell width being small compared to R, and neglects terms of order $\mathrm{erfc}(R^2/\sigma^2)$, where $\mathrm{erfc}(x)$ is the complementary error function. Neglecting terms of order $\mathrm{erfc}(R^2/2\sigma^2)$, Eqs. (1) and (8) give

$$n(p) = \frac{2\sigma}{\pi^{3/2}p^2(\sigma^2+2R^2)}(p\sigma^2\cos pR + R\sin pR)^2$$
$$\times\exp(-\sigma^2 p^2). \quad (9)$$

The bond length is accurately known from spectroscopic measurements ($R=0.3405$ Å [10]) and the value of σ can be determined from the frequency of molecular vibration. In the vibrational ground state the total kinetic en-

ergy of molecular vibration is $\omega_V/4$ where ω_V is the vibrational frequency. Thus each atom has kinetic energy $\omega_V/8$ and since the potential is assumed harmonic, the momentum distribution is Gaussian with a standard deviation of $\sigma_V=\sqrt{M\omega_V/4}$ [8]. With $\omega_V=516$ meV, $\sigma_V=5.577$ Å^{-1} and the mean square displacement of the atom from its mean position along the bond is $\sigma^2/2=1/4\sigma_V^2$; thus $\sigma=0.1269$ Å. With these values of σ and R, the approximations involved in the derivation of Eq. (9) are accurate to better than 1 part in 10^6.

The functions $J_V(y)$ and $J(y)$, calculated from Eqs. (5), (6), (7), and (9) using the values of σ, R, and σ_T obtained above, are shown in Fig. 3, together with the convolution of $J(y)$ with the average instrument resolution function for the 35°–55° bank of detectors. The solid line in Figs. 1(a)–1(c) is a fit to a convolution of the model $J(y)$ with the resolution function. The only fitting parameters are a scale factor, the position of the distribution, and the polynomial coefficients, which account for the multiple scattering background. The values of σ, R, and σ_T were fixed at the values given above. It can be seen that the model gives excellent agreement with the measurements at all angles. The small shift in the peak position from the expected value at $y=0$ is due to inaccuracies in the IA. The solid line in Fig. 2(a) is the calculated $J(y)$ after convolution with the resolution function —there are no free parameters. The difference between the predictions of the model and the symmetrized data is shown in Fig. 2(b) as the points O. The good agreement between data and calculation suggests that the symmetrization effectively removes the small deviations from the IA which are observed in the data. A fit to the data shown in Fig. 2(a) with R and σ as free parameters gave $R=0.356\pm0.003$ Å and $\sigma=5.70\pm0.03$ Å^{-1}, in good agreement with the values of 0.37 and 5.577 obtained from spectroscopy, although outside the quoted statistical error, due to small systematic errors.

The importance of including the oscillatory terms in Eq. (9) is demonstrated by the predictions of a classical model, which neglects the wave nature of the proton. It

is assumed that the molecule is a classical linear vibrator and that each proton has a Gaussian momentum distribution along the bond. Averaging over all possible directions of the bond axis in space to take account of the isotropy of the sample gives

$$n(p) = \frac{1}{2\pi p^2} n_V(p), \qquad (10)$$

where $n_V(p)$ is the distribution of momentum components along the bond. A calculation using Eqs. (5), (6), (7), and (10) gives the results shown as the dashed line in Fig. 2(a). The difference between the classical and the quantum models is shown as the solid line in Fig. 2(b). The same values of the vibrational and translational kinetic energies were used in both calculations. The difference displays oscillations with a first maximum at $y \approx \pi/2R$. This is well reproduced by the data points ×, which are the difference between the data and the classical prediction. The oscillations in the data are the first observation of interference between the proton and neutron wave functions.

The future applications of NCS measurements from protons and deuterons are very wide. An example is the hydrogen bond where NCS can determine whether the observed bimodal distribution of the proton in hydrogen bonds is the result of statistical or quantum disorder [29]. The information obtained from NCS is qualitatively different from that given by neutron diffraction measurements. The latter determine an infinite time average of the spatial distribution of the proton whereas the former measures the proton wave function on a very short time scale. Thus NCS can distinguish between quantum tunneling and thermally induced hopping of the proton between different sites. One application is to the study of the mechanism of protonic diffusion in metals, semiconductors, and ionic conductors. Another is to the determination of the proton wave function in molecules which undergo rotational tunneling [30]. In the latter case an independent measurement of the molecular center of mass motion can be made by NCS measurements on heavier atoms in the molecule.

The very close agreement between data and calculation in this simplest of protonic condensed matter systems demonstrates that NCS measurements have now reached a high level of accuracy. It shows that wave functions of protons can be determined even in isotropic samples, such as liquids, powders, amorphous materials, and polymers. Much more detailed information about the proton wave function can be obtained from single crystal samples, where NCS allows a model-independent reconstruction of both the proton wave function and the potential well of the proton in three dimensions [29]. Orders of magnitude increases in the accuracy of NCS measurements will soon be produced by improvements in count rate and resolution and it seems certain that future measurements will provide precise and unique information about the short time dynamics of protons in many condensed matter sys-

tems of fundamental physical interest.

[1] P. C. Hohenberg and P. M. Platzmann, Phys. Rev. 152, 198 (1966).

[2] P. M. Platzmann, in Momentum Distributions, edited by R. N. Silver and P. E. Sokol (Plenum, New York, 1989), p. 249.

[3] I. Sick, in Momentum Distributions (Ref. [2]), p. 175.

[4] R. Newton, Scattering Theory of Waves and Particles (Springer, Berlin, 1981).

[5] V. F. Sears, Phys. Rev. B 30, 44 (1984).

[6] J. Mayers, Phys. Rev. B 41, 41 (1990).

[7] R. Hempelmann, D. Richter, and D. L. Price, Phys. Rev. Lett. 58, 1016 (1987).

[8] M. Warner, S. W. Lovesey, and J. Smith, Z. Phys. B 39, 2022 (1989).

[9] R. S. Holt, J. Mayers, and A. D. Taylor, in Momentum Distributions (Ref. [2]), p. 295.

[10] I. F. Silvera, Rev. Mod. Phys. 52, 393 (1980).

[11] R. A. Cowley and A. D. B. Woods, Phys. Rev. Lett. 21, 787 (1968).

[12] O. K. Harling, Phys. Rev. Lett. 24, 1046 (1970).

[13] H. A. Mook, Phys. Rev. Lett. 32, 1167 (1974).

[14] H. A. Mook, Phys. Rev. Lett. 51, 1454 (1983).

[15] P. Martel, E. C. Svensson, A. D. B. Woods, V. F. Sears, and R. A. Cowley, J. Low Temp. Phys. 23, 285 (1976).

[16] T. R. Sosnick, W. M. Snow, and P. E. Sokol, Phys. Rev. B 41, 11 185 (1990).

[17] D. A. Peek, M. C. Schmidt, I. Fujita, and R. O. Simmons, Phys. Rev. B 45, 9671 (1992); 45, 9680 (1992).

[18] H. Rauh and N. Watanabe, Phys. Lett. 100A, 244 (1984).

[19] M. P. Paoli and R. S. Holt, J. Phys. C 21, 3633 (1988).

[20] S. Ikeda, K. Shibata, Y. Nakai, and P. W. Stephens, J. Phys. Soc. Jpn. 61, 2619 (1992).

[21] W. Langel, D. L. Price, R. O. Simmons, and P. E. Sokol, Phys. Rev. B 38, 11 275 (1988).

[22] K. W. Herwig, J. L. Gavilano, M. C. Schmidt, and R. O. Simmons, Phys. Rev. B 41, 96 (1990).

[23] S. W. Lovesey, Theory of Neutron Scattering from Condensed Matter (Oxford Univ. Press, New York, 1987).

[24] G. B. West, in Momentum Distributions (Ref. [2]), p. 95.

[25] J. Mayers and A. C. Evans, Rutherford Laboratory Report No. RAL-91-048, 1991 (unpublished).

[26] P. A. Seeger, A. D. Taylor, and R. M. Brugger, Nucl. Instrum. Methods Phys. Res., Sect. A 240, 98 (1985).

[27] C. G. Windsor, Pulsed Neutron Scattering (Taylor & Francis, London, 1981).

[28] C. Andreani, G. Baciocco, R. S. Holt, and J. Mayers, Nucl. Instrum. Methods Phys. Res., Sect. A 276, 297 (1989).

[29] G. Reiter and R. N. Silver, Phys. Rev. Lett. 54, 1047 (1985).

[30] W. Press, Single Particle Rotations in Molecular Crystals (Springer, Berlin, 1981).